

Observation of Floquet Chern insulators of light

Jicheng Jin^{1,4}, Li He^{1,4}, Jian Lu^{1,3}, Lin Chang², Chen Shang², John E. Bowers², Eugene J. Mele¹,
Bo Zhen¹

¹*Department of Physics and Astronomy, University of Pennsylvania, Philadelphia, Pennsylvania
19104, USA*

²*Department of Electrical and Computer Engineering, University of California, Santa Barbara,
California, USA*

³*Current affiliation: Cymer Inc., 17075 Thornmint Ct. San Diego, California 92127, USA*

⁴*These authors contributed equally: Jicheng Jin, Li He.*

Abstract

The field of topological photonics studies unique and robust photonic systems that are immune to defects and disorders due to the protection of their underlying topological phases. Mostly implemented in static systems, the studied topological phases are often defined in linear photonic band structures. In this study, we experimentally demonstrate Floquet Chern insulators in periodically driven nonlinear photonic crystals, where the topological phase is controlled by the polarization and the frequency of the driving field. Mediated by strong material nonlinearity, our system enters what we call the “strong Floquet coupling regime”, where the photonic Floquet bands cross and open new energy gaps with non-trivial topology as observed in our transient sum-frequency gen-

eration measurements. Our work offers new opportunities to explore the role of classical optical nonlinearity in topological phases and their applications in nonlinear optoelectronics.

Introduction

One of the key concepts in the study of light-matter interaction is the strong-coupling regime^{1,2}, where light and matter degrees of freedom (e.g., atoms³, excitons^{4,5}, phonons⁶, plasmons⁷, and magnons⁸) hybridize and form new quasiparticles known as polaritons, giving rise to a plethora of fascinating phenomena⁹. Beyond these linear systems in static, a new realm exists in periodically driven (i.e., Floquet¹⁰) nonlinear optical materials, where two orthogonal eigenmodes of the linear system strongly interact, mediated by an external driving field and material nonlinearity. A characteristic Floquet setup can be a multi-mode optical resonator made of parametric-nonlinear materials periodically driven by a monochromatic field, causing the underlying linear resonances to interact. When the nonlinear interaction is strong enough to overcome the losses, the system enters, what we call, the “strong Floquet coupling” regime, where the linear resonances renormalize into new Floquet eigenmodes, often accompanied by phenomena like normal mode splittings as observed in isolated resonators¹¹⁻¹³.

The theoretical framework of Floquet physics is also applicable to spatially periodic materials and structures, such as crystalline solids and photonic crystals (PhCs), leading to the formation of Floquet-Bloch bands that are bounded in both energy and momentum. In the strong Floquet coupling regime, new energy gaps (i.e., Floquet gaps) are opened with their topological properties

determined by the driving field, paving a new path to engineer band topology^{14–17}.

Floquet topological phases have been studied in various wave systems^{18–20}, with most demonstrations in electronics^{21–24}, which exhibit fundamental differences from their photonic counterparts¹⁸. Whether particle number is conserved or not gives rise to many of these distinctions. For example, the conservation of charges in a closed system guarantees a Hermitian eigenvalue problem. Accordingly, electronic Floquet topological phases are always concerned with the band topology of real energy spectra. In contrast, the number of photons is not necessarily conserved in nonlinear optical processes (e.g., in an optical parametric amplifier, both signal and idler photon number increase due to high-energy pump photons, $\omega_{\text{sig}} + \omega_{\text{idl}} = \omega_{\text{pump}}$) and the corresponding Floquet eigenvalue problems are necessarily non-Hermitian^{25,26}. Moreover, even in scenarios with guaranteed real spectra²⁶ (e.g., when pump photons have low energies, $\omega_{\text{sig}} - \omega_{\text{idl}} = \omega_{\text{pump}}$), photons can be dissipated through the intrinsic loss of Floquet eigenmodes (via material absorption or radiation into free space modes), in contrast to periodically driven electronic systems where interacting electrons will keep absorbing energies from the driving field and dissipating energies to other system degrees of freedom, which eventually leads to an infinite-temperature state where no topological features can be observed¹⁵. From an experimental point of view, electronic bands can directly interact with the driving electromagnetic field (e.g., via electric-dipole transitions), while photons rarely interact, except through material nonlinearity that is generally weak. Consequently, in practice, one needs PhC modes with long lifetime to observe Floquet topological phases of light.

Here we experimentally demonstrate Floquet Chern insulators of light by driving a nonlin-

ear PhC into the strong Floquet coupling regime and opening Floquet gaps with non-trivial Chern numbers. The AlGaAs-on-isolator platform is chosen for its large quadratic nonlinear susceptibilities and low losses in the near-infrared regime, enabling both strong Floquet couplings and long resonance lifetime. We start by presenting the Floquet band structures and their corresponding topological properties under driving fields of different polarizations. The Floquet band dispersions are experimentally probed in transient sum-frequency generation, featuring non-trivial dependence on the drive. Fitting these experimental results to a Floquet temporal coupled mode theory we develop, we extract the nonlinear interaction strength between photonic bands and confirm that it indeed overcomes all the losses combined and our system has reached the strong Floquet coupling regime. Finally, we experimentally reconstruct our Floquet band structures, showing good agreement with simulation, and demonstrate the emergence of Floquet Chern insulators under circularly polarized drive.

Main text

First, we present the theoretical framework and the design of our optical Floquet Chern insulator. We then show our linear and nonlinear optical measurement results, which include Floquet bands and band-gaps measured under driving fields of various polarizations and frequencies.

Floquet Chern insulators of light identified by symmetry indices We begin by introducing the exact configuration of our Floquet Chern insulator, consisting of a nonlinear PhC driven by an external laser (Fig. 1a). The nonlinear PhC consists of a square lattice of air cylindrical holes in

an $\text{Al}_{0.28}\text{Ga}_{0.72}\text{As}$ slab on a SiO_2 substrate. The calculated linear band structure (Fig. 1b) shows the three bands of relevance, including one at higher frequencies and two at lower frequencies forming a quadratic degeneracy at Γ . Along k_x and k_y axis, the two low-frequency bands can be distinguished by their distinctive mirror-symmetry properties: the red (blue) one always radiates y -polarized (x -polarized) light in the far field. See Methods for more details on the material parameters used in the numerical simulation. When the nonlinear PhC is periodically driven in time by an external laser at an angular frequency Ω , the linear band structure is replaced by Floquet band structures. Specifically, due to the quadratic nonlinearity of AlGaAs, the photonic bands produce sidebands (e.g., dashed lines) that shift up and down by multiples of Ω in the spectrum, similar to sum- and difference-frequency generation processes.

The polarization and frequency of the driving field determine how these sidebands interact and re-normalize into Floquet bands, as well as their symmetries and topologies. For instance, a x -polarized drive preserves both x - and y -mirror symmetries of the system and can only couple two of the three photonic bands (red and black), but not all three (Fig. 1c). This can also be intuitively understood by analyzing the nonlinear susceptibility of AlGaAs, $\chi_{xyz}^{(2)}$. Under a x -polarized drive, the E_y component of the red band is coupled to the E_z component of the black band inside the PhC, while neither of them couples to the E_x component of the blue band. As a result, under a x -polarized drive at frequency $\Omega c/2\pi a = 0.15$, a Floquet gap is opened along k_x axis, where the red and yellow bands cross, but no gap is opened along k_y , where the blue and yellow bands cross. The resulting Floquet bands remain connected in the spectrum (i.e., gapless) through two linear (Dirac) degeneracies along k_y . In contrast, a circularly polarized drive ($\hat{x} + i\hat{y}$)

at the same frequency breaks both mirror symmetries and couples all three photonic bands. The resulting Floquet band structure features a full gap (shaded in gray in Fig. 1c) between the top and the two bottom Floquet bands, which is topological and characterized by a non-zero Chern number $C = 1$.

The Chern number of the Floquet gap is confirmed in three ways. First, it is calculated by integrating the Berry curvature of the Floquet bands over the entire Brillouin zone, following our previous derivation²⁶. More details on the Berry curvature calculations are provided in Section I in the Supplementary Information. The Chern number is then confirmed through the bulk-edge correspondence in a super-cell geometry, where a pair of unidirectional Floquet chiral edge states are observed at the edge of the Floquet Chern insulator. More details on the Floquet chiral edge states are provided in Section II in the Supplementary Information.

In a most straightforward way, the non-trivial topology is also confirmed using the symmetry indices at high-symmetry k -points. Specifically, the driving field, regardless of its polarization, always preserves the space-time compound symmetry²⁷ of $\tilde{C}_2 = C_2^z \hat{T}_{T/2}$. Here, C_2^z is the 180-degree spatial rotation around the z -axis, and $\hat{T}_{T/2}$ is the temporal translation by half of the modulation period ($T = 2\pi/\Omega$). Four points in the k -space (Γ, X, Y, M) are invariant under \tilde{C}_2 , and their \tilde{C}_2 index must be ± 1 since $\tilde{C}_2^2 = 1$. The Chern number of the highest-frequency Floquet band can be related to its \tilde{C}_2 indices at these four points:

$$e^{i\pi C} = \tilde{C}_2(\Gamma)\tilde{C}_2(X)\tilde{C}_2(Y)\tilde{C}_2(M). \quad (1)$$

Under a linearly polarized (e.g., x -) drive, the Floquet bands always remain gapless, preventing

one from defining a Chern number using Eq. 1. In contrast, the Floquet gap is fully opened under a circular drive, and the gap Chern number can be further simplified as $e^{i\pi C} = \tilde{C}_2(\Gamma)\tilde{C}_2(M) = -1$, confirming that the Floquet gap is indeed topologically non-trivial ($C \neq 0$). This is consistent with the fact that time-reversal symmetry is preserved under a linear polarized drive but broken under an elliptically (e.g., circularly) polarized drive in AlGaAs²⁷. Section III in the Supplementary Information provides more details on the symmetry indices and how topological phase transition can happen in the polarization space of the driving field in this particular system.

Linear band characterizations of AlGaAs PhCs The AlGaAs PhCs (Fig. 2a) are fabricated following the procedures of wafer bonding, electron-beam lithography, and reactive ion etching (see Methods for more details). The linear band structure is measured through angle- and polarization-resolved linear reflection spectroscopy (Fig. 2b), which shows the three photonic bands of interest and their corresponding far-field polarizations (x or y) along the k_x and k_y axis. By fitting the reflection data to a temporal coupled mode theory model²⁸, the linear band structure is reconstructed (Fig. 2c), including both the resonance frequencies $\text{Re}(\omega)$ and the decay rates $\text{Im}(\omega)$. Section IV in the Supplementary Information provides more details on the linear temporal coupled mode theory and the fitting procedures.

Observation of nonlinear Floquet bands To characterize the Floquet band structure, a pump-probe setup is developed (Fig. 3a). The nonlinear PhC is periodically driven by a narrow-band pump field at wavelength λ_P (pulse duration ~ 1.8 picoseconds) and incidents from the normal direction. Meanwhile, the PhC resonances are excited by a broadband probe beam (~ 169 fem-

toseconds) centered at wavelength λ_B . Both the pump and probe lasers are seeded from the same oscillator and amplifier (Pharos, Light Conversion) to minimize relative time jitter. The pump and probe beams are properly delayed in time to achieve optimal temporal overlap on the sample. The pump beam, probe beam, and quadratic nonlinearity of AlGaAs work together to populate the Floquet bands, whose far-field radiation is captured by the same lens and recorded with a monochromator and a 2D CCD. This setup can measure both transient sum-frequency generation (SFG) at wavelength λ_S and transient reflection signals at λ_B , separable via a dichroic mirror. Section V in the Supplementary Information provides more details on the nonlinear characterization setup.

Examples of our measured Floquet bands are shown in Fig. 3b. Here, the mid-infrared pump field ($\lambda_P \approx 3\mu\text{m}$) is x -polarized. The near-infrared probe field ($\lambda_B \approx 1\mu\text{m}$) is y -polarized, exciting the red band in Fig. 1b and 2c. Strong SFG emission is observed from the sidebands in the visible regime ($\lambda_S \approx 760\text{ nm}$). Meanwhile, the transient SFG spectrum is strongly modulated by the linear photonic resonances (dashed blue line), corresponding to the black band in Fig. 1b and Fig. 2c. As expected, the sideband frequency (color map) keeps increasing with the pump frequency — as λ_P decreases from $3.2\mu\text{m}$ to $3.02\mu\text{m}$ — while the frequency of the linear resonance (dashed blue line) remains largely unchanged.

Reaching the strong Floquet coupling regime We experimentally determine the nonlinear coupling strength between photonic bands and confirm that our system has reached the strong Floquet coupling regime, opening Floquet gaps in the spectrum. To quantify the coupling strength g , we

analyze the intensity dependence of the transient SFG on pump power (Fig. 4a). In these measurements, the pump wavelength is fixed at $\lambda_P = 3.05\mu\text{m}$, and we record the intensity of the transient SFG at 760nm, where the two Floquet bands cross (highlighted by a white box in Fig. 3b), as the pump power increases from 0 to 45mW. As shown, the transient SFG intensity, I_{SFG} , reaches its maximum value of $I_{\text{SFG}}^{\text{max}}$ when the pump power is at $P = 21\text{mW}$ and is reduced at lower or higher pump. Similar power dependence has been observed in previous literature on resonance-based SFG¹² and is also captured by our Floquet temporal coupled mode theory. Specifically, I_{SFG} can be expressed as:

$$\frac{I_{\text{SFG}}}{I_{\text{SFG}}^{\text{max}}} = \frac{4C}{(1 + C)^2}, \quad (2)$$

where C is the cooperativity of the system, defined as $C = g^2/(\gamma_1\gamma_2)$. Meanwhile, $\gamma_{1,2} = \text{Im}(\omega_{1,2})$, which equals half the resonance linewidth, represents the loss of the two involved resonances, respectively. Following Eq. 2, I_{SFG} reaches its maximum under the condition of $C = 1$, which is satisfied at $P = 21\text{mW}$.

Both coupling strength g and cooperativity C increase with pump power: $g \propto \sqrt{P}$ and $C \propto P$. Our largest experimentally achieved coupling strength is $g_{\text{max}}/2\pi = 185\text{GHz}$ and the highest cooperativity is $C_{\text{max}} = 2.06$, both under the pump power of $P = 45\text{mW}$ (Fig. 4b). This nonlinear coupling strength is larger than all losses combined in our system, $g_{\text{max}}/2\pi > \sqrt{(\gamma_1^2 + \gamma_2^2)/2}/2\pi = 129.1\text{GHz}$, which proves that our system has entered the strong Floquet coupling regime, even by the most stringent criteria used in the literature of cavity quantum electrodynamics^{15,29–31} Section VI and VII in the Supplementary Information provides more details on the Floquet temporal coupled mode theory model and the fitting procedure.

Observation of nonlinear Floquet Chern insulators The complete Floquet band structure can be reconstructed by fitting the experimental data (linear reflection and transient SFG spectra) to our Floquet temporal coupled mode theory and extracting the nonlinear coupling strength over a wide range of momenta. As a result, the reconstructed Floquet band structure under a x -polarized driving field is shown in Fig. 5a, which features a Floquet gap along the k_x axis as well as a pair of linear (Dirac) degeneracies along the k_y axis — both features are in good agreement with our theoretical prediction in Fig. 1b and the experimental results in Fig. 4b. In contrast, the reconstructed Floquet band structure under a circularly polarized drive is fully gapped along both directions (Fig. 5b). The resulting system is a Floquet Chern insulator, corresponding to our calculations in Fig. 1c. Section IX in the Supplementary Information provides more details on the reconstruction of the Floquet band structure from our Floquet temporal coupled mode theory.

Discussion and conclusion

Our pump-probe setup is designed to maximize Floquet physics arising from quadratic nonlinearity while minimizing the impact of unwanted nonlinear processes. For example, our pump pulse duration is chosen to be about 1.8 picoseconds, which is too short for thermal nonlinearities to take effect. Meanwhile, this time scale is comparable to the lifetime of the photonic resonances involved, ensuring strong interactions between the pump field and the resonances. Our pump field (~ 0.3 GV/m) guarantees quadratic nonlinearities to dominate over other (e.g., cubic) nonlinearities in our system. Finally, our SiO₂ substrate is chosen to be JGS3 to avoid MIR pump absorption and cubic nonlinearity.

In current our experimental results, the largest achieved nonlinear cooperativity $C_{\max} \approx 2.1$ is limited by two factors. First, our peak pump field is close to the damage threshold of AlGaAs at this wavelength for this pulse duration. To further improve the damage threshold, an even lower-frequency driving field (possibly in the far-infrared regime) is needed. On the other hand, the material absorption in AlGaAs beyond its direct bandgap at longer wavelengths limits the lifetime of the resonances, which is consistent with the literature.³². Changing to another material with lower absorption losses but comparable nonlinearities and damage thresholds can be beneficial in further improving the resonance lifetime and, therefore, nonlinear cooperativity.

In summary, we report the experimental observation of Floquet Chern insulators in driven nonlinear photonic crystals, where both the Floquet band structures and their topological properties can be controlled by the driving field. Our system enters the strong Floquet coupling regime, as the nonlinear coupling strength, mediated by the strong pump field and material nonlinearity, exceeds all loss mechanisms combined. The Floquet band structures are experimentally reconstructed from our linear and nonlinear experimental results, featuring Floquet energy gaps due to the pump and showing good agreement with simulation results. Our work paves the way for future explorations of Floquet topological phases in driven nonlinear systems and opens new possibilities in implementing on-chip topologically robust photonic devices and energy-efficient non-reciprocal devices.

Methods

Numerical simulation details. Without a driving field, the PhC band structure is calculated using a finite element method similar to our previous calculations²⁶. The refractive index of $\text{Al}_{0.28}\text{Ga}_{0.72}\text{As}$ is set to be $n = 3.47$ and 3.3 at 760nm and $1\mu\text{m}$, respectively. The refractive index of SiO_2 substrate is set to be $n = 1.46$. For Floquet band calculations, the quadratic nonlinearity of $\text{Al}_{0.28}\text{Ga}_{0.72}\text{As}$ is $\chi_{xyz}^{(2)} = \chi_{yzx}^{(2)} = \chi_{zxy}^{(2)} = 200\text{pm/V}$, which is consistent with previous literature³³⁻³⁵

Sample fabrication. An AlGaAs wafer with an 85 nm thick $\text{Al}_{0.28}\text{Ga}_{0.72}\text{As}$ film and a 500nm thick $\text{Al}_{0.8}\text{Ga}_{0.2}\text{As}$ sacrificial layer is grown on a $500\mu\text{m}$ thick GaAs substrate. The thin film side is flip-bonded onto a SiO_2 substrate, which is chosen to be JGS3 to minimize MIR absorption and cubic nonlinearity. The GaAs substrate is then removed through mechanical polishing and wet etching with $\text{H}_2\text{O}_2:\text{NH}_4\text{OH}$ (30:1). We then remove the $\text{Al}_{0.8}\text{Ga}_{0.2}\text{As}$ sacrificial layer with dilute hydrofluoric 2.5% acid and deposit a 5nm -thick Al_2O_3 layer through ALD for passivation. For lithography, the chips are spin-coated with a 300nm -thick ZEP 520A and the patterns are defined with Raith EBPG 5200, with a cold development at -6°C in o-xylene. The pattern on the photoresist is then transferred onto the AlGaAs layer by ICP etching (Oxford Corba) with a mixture of $\text{BCl}_3/\text{Cl}_2/\text{Ar}$. In the end, the sample is passivated with a 5nm -thick layer of Al_2O_3 by ALD.

Optical measurement setups. All presented experimental results are from angle-resolved and polarization-resolved spectroscopy measurements. The sample is mounted onto a JGS3 substrate with anti-reflection coating with optical gel to eliminate spectral fringes due to multiple reflections.

The entire sample is then placed at the focal plane of an achromatic lens with a focal length of 4cm. The confocal setup converts the momentum space of the PhC into real space, which is then mapped onto the entrance slit of the monochromator using relay optics. Angle- and polarization-resolved spectrum along one momentum direction is directly read out with a 2D CCD. By scanning the position of the entrance slit, measurements along both momentum directions can be performed. The etaloning effect of the CCD is not significant around 760nm but is clearly visible near $1\mu\text{m}$. It is calibrated out following standard procedures^{36,37}. Different light sources are used for different measurements. For linear band characterization, a femtosecond optical parametric amplifier is used. For nonlinear measurements, a picosecond MIR optical parametric amplifier is used to drive the sample, while a NIR femtosecond probe laser is used to excite the resonances.

Data availability The data within this paper are available from the corresponding author upon request.

Acknowledgments This work was partly supported by the U.S. Office of Naval Research (ONR) through grant N00014-21-1-2703, the Army Research Office under award contract W911NF-19-1-0087, and DARPA under agreement HR00112220013. Work by E.J.M is supported by the Department of Energy under grant DE-FG02-84ER45118.

Author Contributions J.J., L.H., J.L., and B.Z. conceived the project. J.J. and L.H. performed numerical simulations. J.J. fabricated the sample assisted by L.H. L.C. C.S. and J.B. provided bonded wafers. J.J., L.H. and J.L. performed the experiment. J.J., L.H., and B.Z. wrote the paper with input from all authors. All authors discussed the results. B.Z. supervised the project.

Competing interests The authors declare no competing interest.

Correspondence Correspondence should be addressed to B.Z. (email: bozhen@sas.upenn.edu).

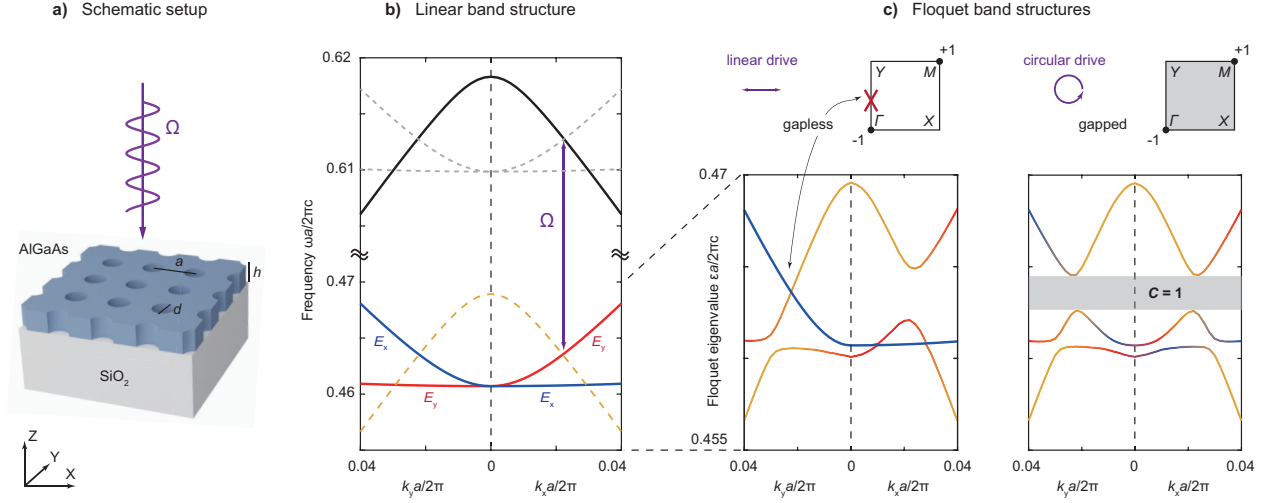


Fig. 1 | Floquet Chern insulators of light identified by symmetry indices. **a.** Schematic of a nonlinear (AlGaAs) photonic crystal (PhC) periodically driven by an external laser at frequency Ω . The geometric parameters are $h/a = 0.18$ and $d/a = 0.2$. **b.** The linear band structure features three bands of relevance: one at higher frequencies (black line) and the other two at lower frequencies (red and blue). **c.** A x -polarized drive couples the photonic bands via the quadratic nonlinearity of AlGaAs along the k_x axis, but not along the k_y axis, leading to a pair of linear (Dirac) degeneracies. **d.** A circularly polarized drive opens a full Floquet gap (shaded in gray), resulting in a Floquet Chern insulator of light. The topological nature of the highest-frequency Floquet band is confirmed by its \tilde{C}_2 symmetry indices: -1 at Γ and $+1$ at M .

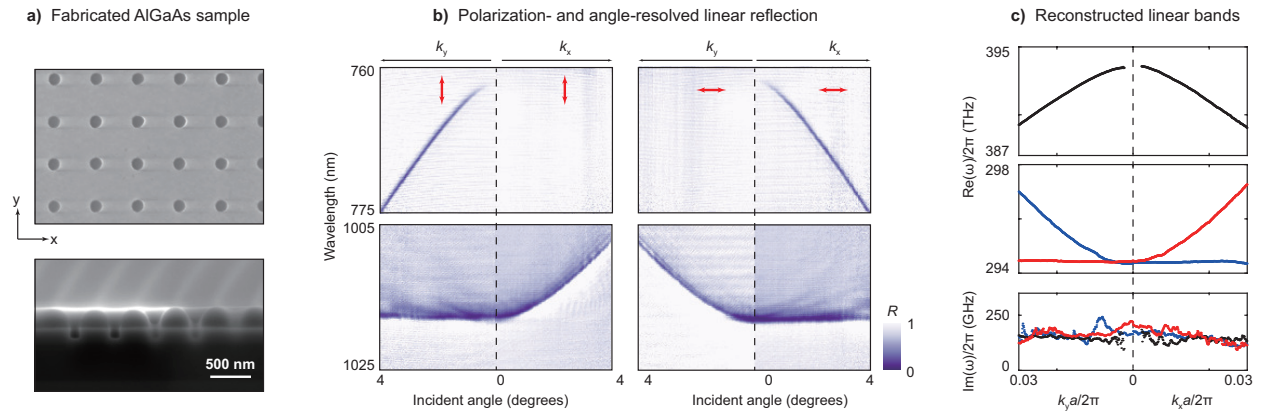


Fig. 2 | Linear characterization of AlGaAs PhCs. **a.** SEM images of fabricated AlGaAs PhCs with $a = 465$ nm, $d = 100$ nm, and $h = 85$ nm. **b.** Angle-resolved linear reflection measurements along the k_x and k_y axis under vertically and horizontally polarized excitations, featuring the three bands of interest. **c.** Experimentally extracted resonance frequencies and decay rates of the three photonic bands from linear reflection measurements.

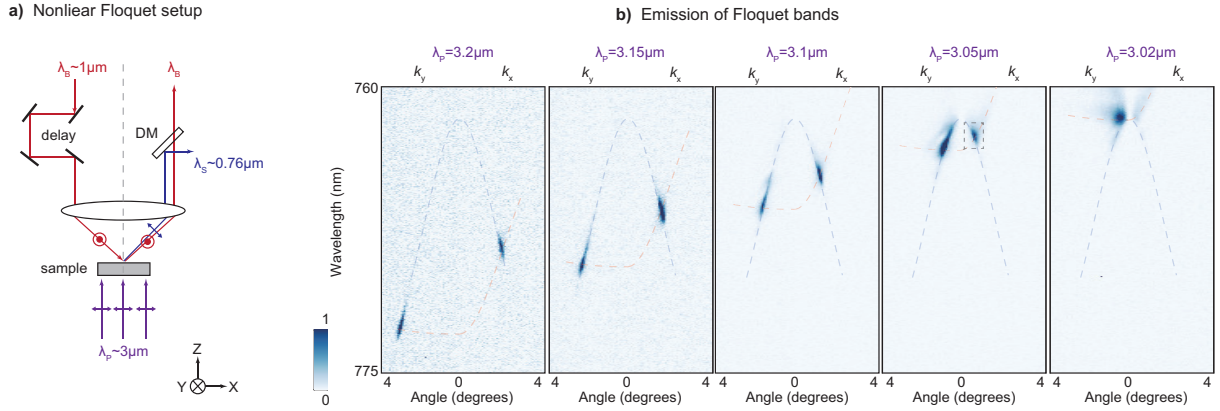


Fig. 3 | Observation of nonlinear Floquet bands. **a**, Schematics of the nonlinear Floquet measurement setup. A x -polarized pump laser (purple) with a wavelength λ_P periodically drives the nonlinear PhC, while the probe beam (λ_B , red) excites the linear resonances. Angle-resolved transient sum-frequency generation (λ_S , blue) is recorded using a monochromator and a 2D CCD. **b**, The transient sum-frequency generation spectra clearly show the dispersion of the Floquet bands (dashed lines). Their frequencies increase with the pump frequency, as λ_P changes from $3.2\mu\text{m}$ to $3.02\mu\text{m}$. Meanwhile, the linear band remains fixed in frequency (dashed blue line). DM, dichroic mirror.

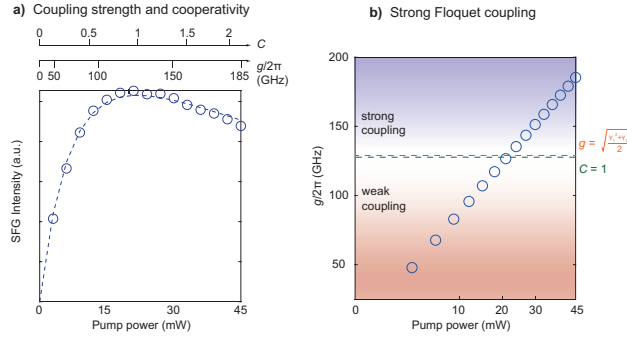


Fig. 4 | Reaching the strong Floquet coupling regime. **a**, Both nonlinear coupling strength between photonic resonances (g) and cooperativity (C) are extracted from measured transient SFG intensity I_{SFG} under different pump powers (circles). **b**, The nonlinear coupling strength g increases with the pump power and reaches its maximum value of $g_{\max}/2\pi = 185\text{GHz}$ under the pump power of $P = 45\text{mW}$. This nonlinear coupling strength exceeds all loss mechanisms combined (different definitions are shown in dashed lines), proving that our system enters the strong Floquet coupling regime and new Floquet gaps are opened.

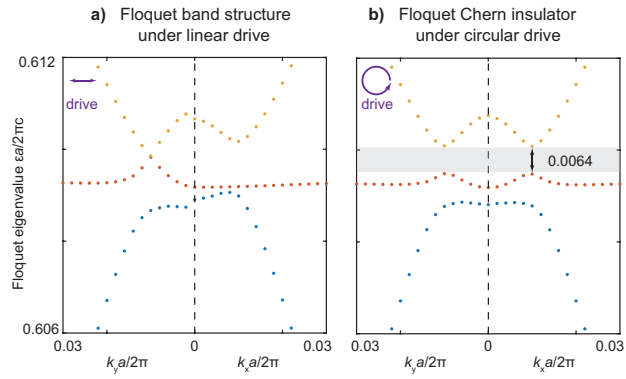


Fig. 5 | Observation of Floquet Chern insulators of light. **a.** The Floquet band structures are experimentally reconstructed from linear and nonlinear spectra. Under a x -polarized drive, the Floquet band structure features a Floquet gap along k_x and a Dirac point along k_y . **b.** In contrast, under a circularly polarized drive, the Floquet gap is opened along both axes (shaded in gray), corresponding to the nonlinear Floquet Chern insulator in Fig. 1c.

References

1. Thompson, R. J., Rempe, G. & Kimble, H. J. Observation of normal-mode splitting for an atom in an optical cavity. *Physical Review Letters* **68**, 1132–1135 (1992).
2. Chang, D. E., Douglas, J. S., González-Tudela, A., Hung, C.-L. & Kimble, H. J. Colloquium: Quantum matter built from nanoscopic lattices of atoms and photons. *Reviews of Modern Physics* **90**, 031002 (2018).
3. Douglas, J. S. *et al.* Quantum many-body models with cold atoms coupled to photonic crystals. *Nature Photonics* **9**, 326–331 (2015).
4. Zhang, L., Gogna, R., Burg, W., Tutuc, E. & Deng, H. Photonic-crystal exciton-polaritons in monolayer semiconductors. *Nature Communications* **9**, 713 (2018).
5. Deng, H., Haug, H. & Yamamoto, Y. Exciton-polariton bose-einstein condensation. *Reviews of Modern Physics* **82**, 1489–1537 (2010).
6. Faust, W. L. & Henry, C. H. Mixing of visible and near-resonance infrared light in gap. *Physical Review Letters* **17**, 1265–1268 (1966).
7. Zhang, J., Zhang, L. & Xu, W. Surface plasmon polaritons: Physics and applications. *Journal of Physics D: Applied Physics* **45**, 113001 (2012).
8. Camley, R. E. & Mills, D. L. Surface polaritons on uniaxial antiferromagnets. *Physical Review B* **26**, 1280–1287 (1982).

9. Basov, D. N., Fogler, M. M. & García de Abajo, F. J. Polaritons in van der waals materials. *Science* **354**, aag1992 (2016).
10. Dittrich, T. *et al.* *Quantum transport and dissipation*, vol. 3 (Wiley-Vch Weinheim, 1998).
11. Xu, J. *et al.* Floquet cavity electromagnonics. *Physical Review Letters* **125**, 237201 (2020).
12. Guo, X., Zou, C.-L., Jung, H. & Tang, H. X. On-chip strong coupling and efficient frequency conversion between telecom and visible optical modes. *Physical Review Letters* **117**, 123902 (2016).
13. Dobrindt, J. M., Wilson-Rae, I. & Kippenberg, T. J. Parametric normal-mode splitting in cavity optomechanics. *Physical Review Letters* **101**, 263602 (2008).
14. Hasan, M. Z. & Kane, C. L. Colloquium: Topological insulators. *Reviews of Modern Physics* **82**, 3045–3067 (2010).
15. Rudner, M. S. & Lindner, N. H. Band structure engineering and non-equilibrium dynamics in floquet topological insulators. *Nature Reviews Physics* **2**, 229–244 (2020).
16. Peterson, C. W., Li, T., Benalcazar, W. A., Hughes, T. L. & Bahl, G. A fractional corner anomaly reveals higher-order topology. *Science* **368**, 1114–1118 (2020).
17. Hafezi, M., Mittal, S., Fan, J., Migdall, A. & Taylor, J. M. Imaging topological edge states in silicon photonics. *Nature Photonics* **7**, 1001–1005 (2013).
18. Rechtsman, M. C. *et al.* Photonic floquet topological insulators. *Nature* **496**, 196–200 (2013).

19. Lu, J., He, L., Addison, Z., Mele, E. J. & Zhen, B. Floquet topological phases in one-dimensional nonlinear photonic crystals. *Physical Review Letters* **126**, 113901 (2021).
20. Zhu, W., Xue, H., Gong, J., Chong, Y. & Zhang, B. Time-periodic corner states from floquet higher-order topology. *Nature Communications* **13**, 11 (2022).
21. Wang, Y. H., Steinberg, H., Jarillo-Herrero, P. & Gedik, N. Observation of floquet-bloch states on the surface of a topological insulator. *Science* **342**, 453–457 (2013).
22. McIver, J. W. *et al.* Light-induced anomalous hall effect in graphene. *Nature Physics* **16**, 38–41 (2020).
23. Zhou, S. *et al.* Pseudospin-selective floquet band engineering in black phosphorus. *Nature* **614**, 75–80 (2023).
24. Ito, S. *et al.* Build-up and dephasing of floquet–bloch bands on subcycle timescales. *Nature* 1–6 (2023).
25. Winn, J. N., Fan, S., Joannopoulos, J. D. & Ippen, E. P. Interband transitions in photonic crystals. *Physical Review B* **59**, 1551–1554 (1999).
26. He, L. *et al.* Floquet chern insulators of light. *Nature Communications* **10**, 4194 (2019).
27. Jin, J., He, L., Lu, J., Mele, E. J. & Zhen, B. Floquet quadrupole photonic crystals protected by space-time symmetry. *Physical Review Letters* **129**, 063902 (2022).

28. Suh, W., Wang, Z. & Fan, S. Temporal coupled-mode theory and the presence of non-orthogonal modes in lossless multimode cavities. *IEEE Journal of Quantum Electronics* **40**, 1511–1518 (2004).
29. Peng, B., Özdemir, Ş. K., Chen, W., Nori, F. & Yang, L. What is and what is not electromagnetically induced transparency in whispering-gallery microcavities. *Nature Communications* **5**, 5082 (2014).
30. Reithmaier, J. P. *et al.* Strong coupling in a single quantum dot–semiconductor microcavity system. *Nature* **432**, 197–200 (2004).
31. Berman, P. R. *Cavity quantum electrodynamics* (1994).
32. Michael, C. P. *et al.* Wavelength- and material-dependent absorption in gaas and algaas microcavities. *Applied Physics Letters* **90**, 051108 (2007).
33. Chang, L. *et al.* Strong frequency conversion in heterogeneously integrated gaas resonators. *APL Photonics* **4**, 036103 (2019).
34. Chang, L. *et al.* Ultra-efficient frequency comb generation in algaas-on-insulator microresonators. *Nature Communications* **11**, 1331 (2020).
35. Zhu, D. *et al.* Integrated photonics on thin-film lithium niobate. *Advances in Optics and Photonics* **13**, 242–352 (2021).

36. Sanz-Arranz, A., Manrique-Martinez, J. A., Medina-Garcia, J. & Rull-Perez, F. Amorphous zinc borate as a simple standard for baseline correction in raman spectra: Amorphous zinc borate as raman standard. *Journal of Raman Spectroscopy* **48**, 1644–1653 (2017).
37. Massie, C., Chen, K. & Berger, A. J. Calibration technique for suppressing residual etalon artifacts in slit-averaged raman spectroscopy. *Applied Spectroscopy* **76**, 255–261 (2022).